IEEE Access
Multidisciplinary | Rapid Review | Open Access Journal

Received 16 December 2023, accepted 9 January 2024, date of publication 18 January 2024, date of current version 29 January 2024.

Digital Object Identifier 10.1109/ACCESS.2024.3355435

RESEARCH ARTICLE

Flexible Design Method for Multifunctional Filtering Diplexers Integrated With Single-Pole Double-Throw Switches

CHI-FENG CHEN, (Member, IEEE), YI-FANG TSAI, BAI-HONG CHEN, RUO-YIN YANG, AND YU-SHENG ZENG

Department of Electrical Engineering, Tunghai University, Taichung City 40704, Taiwan

Corresponding author: Chi-Feng Chen (cfchen@thu.edu.tw)

This work was supported in part by the Ministry of Science and Technology, Taiwan, under Grant MOST 110-2221-E-029-013; and in part by the National Science and Technology Council, Taiwan, under Grant NSTC 112-2221-E-029-009.

ABSTRACT This paper presents a novel design method for multifunctional filtering diplexers integrated with single-pole double-throw switches having three operating modes: Modes 1–3. Modes 1 and 2 involve the operation of switchable filters with different frequencies, which are suitable for time-division duplexing (TDD) systems. Mode 3 involves the operation of switchable diplexers, which are suitable for TDD and frequency-division duplexing (FDD) systems. The proposed design method is based on distributed coupling technology and can thus offer a high degree of design flexibility, particularly in terms of controlling the filter order, bandwidth, and number of channels. To demonstrate the feasibility and design flexibility of the proposed method, it was used to design and fabricate second- and fourth-order multifunctional diplexers; the designed diplexers were then assessed through electromagnetic simulations and experimental measurements. The simulation results were in good agreement with the experimental results, thereby validating the feasibility and design flexibility of the proposed method. The results indicated that the second- and fourth-order multifunctional diplexers occupied small circuit areas (approximately 0.098 λ_g^2 and 0.198 λ_g^2, respectively). In addition to their multifunctional characteristics and high design flexibility, the multifunctional diplexers exhibited satisfactory performance, including an in-band insertion loss of < 2.5 dB in the ON state, an in-band attenuation of > 42 dB in the OFF state, and a port-to-port isolation of > 48 dB.

INDEX TERMS Bandpass filters (BPFs), diplexers, microstrip, multifunctional components, single-pole double-throw (SPDT) switches.

I. INTRODUCTION

In microwave communication systems, diplexers and multiplexers play a crucial role in controlling multifrequency signals. The circuit structures of diplexers and multiplexers primarily comprise a matching circuit connected to several filters. Such structures must be miniaturized while maintaining sufficient isolation between various channel frequency bands. Such isolation is critical to eliminate interference between transmitter (Tx) and receiver (Rx) signals. Therefore, the design of compact and high-isolation diplexers and multiplexers has become a prominent research topic in recent years. Numerous studies have been conducted on this topic [1], [2], [3], [4], [5], [6], [7], [8], [9], [10]. For example, the researchers in [1] proposed a design approach that primarily involves the use of microstrip lines with high-impedance meander lines to miniaturize diplexers; such miniaturization is achieved using a slow-wave open-loop resonator. Moreover, various techniques have been employed for effectively miniaturizing diplexers, including techniques involving the use of spiral inductor resonators [2], quarter-wavelength resonators [3], stepped-impedance resonators (SIRs) [4]. Common resonator techniques have also been proven to be effective in reducing the circuit area of

The associate editor coordinating the review of this manuscript and approving it for publication was Photos Vryonides.

diplexers and multiplexers [5], [6]. Such techniques can obviate the need for conventional T-junction matching circuits that connect Tx and Rx filters and can reduce the number of resonators required for the entire diplexer and multiplexer circuits, thus substantially reducing the overall circuit size. In addition to circuit miniaturization, achieving high isolation is a crucial objective in the design of diplexers and multiplexers. In [7], the stopband rejection and isolation were achieved using tunable transmission zeros. The researchers in [8] presented a diplexer design approach that involves the use of hybrid resonators that inherently introduce transmission zero characteristics, which can be manipulated to improve isolation across different frequency bands. Recent studies have also focused on developing multiplexers with multiple channel passbands [9], [10].

For further reducing the space occupied by circuits in communication systems and for decreasing manufacturing costs, numerous researchers have focused on integrating the functions of multiple microwave circuits into a single component. For example, the researchers in [11], [12], [13], and [14] have explored the integration of a bandpass filter (BPF) and single-pole double-throw (SPDT) switch into a single component, thereby yielding switchable BPFs. In [11], BPFs have been designed using diode-loaded resonators. In these BPFs, an external bias is used to turn the diodes on or off, thereby altering the resonant frequency of the resonator and consequently switching the passband between the ON and OFF states. In [12], two diodes were added to the feeding structure to enable arbitrary switching between Chebyshev and quasi-elliptic response functions in the BPF. In [13], a compact SPDT switchable BPF based on capacitively loaded multi-coupled line was developed for narrowband applications. Furthermore, in [14], dual-band switchable BPFs applicable in dual-frequency and dual-channel communication systems have been developed.

In modern multiband and multiservice microwave communication systems, diplexers and SPDT switches are key components for meeting the system requirements of time-division duplexing (TDD) and frequency-division duplexing (FDD). In conventional design approaches, diplexers and SPDT switches are designed independently and later interconnected using 50-Ω transmission lines [Fig. 1(a)]. However, these approaches can lead to increased circuit area, elevated transmission loss, and higher manufacturing costs. An effective method for addressing these problems entails integrating the diplexer and SPDT switches into a single component, which is commonly referred to as a switchable diplexer or a diplexer integrated with SPDT switches [Fig. 1(b)]. This integration approach requires only one circuit without compromising system functionality; this approach is practically beneficial in enhancing system compactness, reducing circuit area, and reducing costs. In recent years, several research teams have focused on developing switchable diplexers [15], [16], [17], [18], [19], [20], [21], [22], [23]. For example, in [15], a diplexer

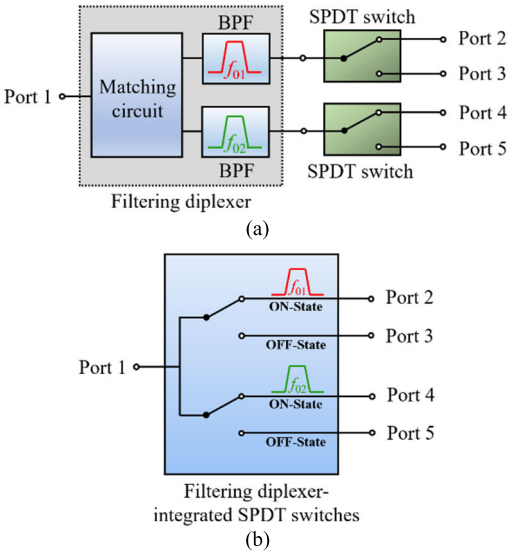

FIGURE 1. Block diagram of a system supporting time-division duplexing and frequency-division duplexing functions: (a) conventional architecture and (b) architecture based on a new switchable diplexer.

was developed using two parallel-coupled BPFs operating in different frequency bands; in this diplexer, diodes are connected to the first-stage resonator, which enables the resonance frequency to be altered by applying an external bias, thus achieving ON–OFF passband switching. In [16], [18], [19], and [21], diplexers have been designed using common resonator techniques; in these diplexers, diodes are connected to the resonator to switch the passband arbitrarily between the ON and OFF states. In [17] and [20], diplexers have been designed using diode-loaded SIRs to achieve passband switching and size miniaturization simultaneously. In [22], a diplexer composed of three sets of dual-mode SIRs was designed; the circuit of this diplexer provides three switching modes. Furthermore, the researchers in [24], [25], and [26] have integrated SPDT switches into multiplexers.

The switchable BPFs developed in [11], [12], [13], and [14] are applicable to only TDD systems, whereas the switchable diplexers developed in [15], [16], [17], [18], [19], [20], [21], [22], and [23] are applicable to only FDD systems. The evolution of modern wireless communication systems, exemplified by the fifth generation (5G), Long-Term Evolution (LTE), and Wi-Fi, necessitates authorized frequency bands capable of supporting both TDD and FDD functions simultaneously. The researchers in [27] presented a method for designing diplexers integrated with SPDT switches by using common fractal stub-loaded resonator. Although this method can help to reduce the circuit size, it presents limitations in the design flexibility of the passband. Therefore, developing innovative multifunctional switchable diplexers is imperative. Accordingly, this paper presents a novel design method for multifunctional filtering diplexers integrated with SPDT switches. This method involves the application of distributed coupling techniques, thus

enhancing design flexibility. Furthermore, to demonstrate the feasibility of the proposed method, it was used to design and fabricate second- and fourth-order multifunctional diplexers; the designed diplexers were then evaluated. The experimental results were in good agreement with predictions obtained from full-wave electromagnetic (EM) simulations. Overall, the developed multifunctional diplexers exhibited advantages such as miniaturization, high selectivity, low loss, and high isolation; thus, these diplexers are highly suitable for modern wireless communication systems that operate with both TDD and FDD functions.

The rest of this paper is organized as follows. Sections III and IV describe the use of the proposed method in designing filtering diplexers integrated with SPDT switches and exhibiting second- and fourth-order bandpass responses, respectively. These sections also detail the procedures involved in validating the feasibility of the proposed method through EM simulations and experimental measurements. Furthermore, Sections IV presents a performance comparison between diplexers designed using the proposed method and state-of-the-art switchable diplexers. Finally, Section IV presents the conclusion of this study.

II. DIPLEXERS INTEGRATED WITH SPDT SWITCHES AND EXHIBITING SECOND-ORDER BANDPASS RESPONSE

The developed multifunctional diplexers have three switchable operating modes (Table 1): Mode 1, in which an SPDT switch is integrated with a BPF centered at f_{01}; Mode 2, in which an SPDT switch is integrated with a BPF centered at f_{02}; and Mode 3, in which SPDT switches are integrated with a filtering diplexer. Modes 1 and 2 are suitable for TDD systems, and Mode 3 is suitable for TDD and FDD systems.

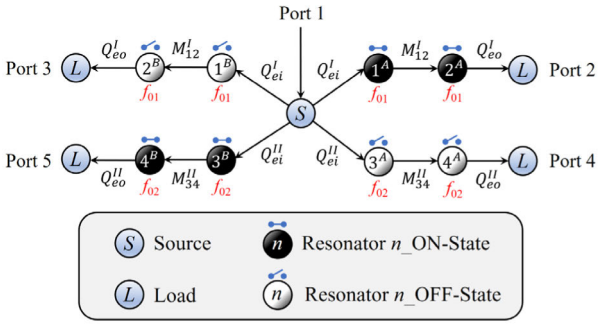

FIGURE 2. Coupling structure of the designed second-order filtering diplexer integrated with SPDT switches.

The proposed design method can be used to design a second-order Chebyshev filtering diplexer integrated with SPDT switches, and Fig. 2 illustrates the coupling structure of this diplexer. The circuit of the aforementioned diplexer functions as a five-port network, with Port 1 serving as the input and Ports 2–5 serving as the outputs. In Fig. 2, Nodes $1^A - 4^A$ and $1^B - 4^B$ represent resonator circuits, and Nodes S and L represent the source and load, respectively. The solid lines connecting the nodes represent the coupling paths. Resonators 1 and 2 are used to construct the passband for Channel I, and their fundamental resonant frequency corresponds to the center frequency of Channel I (f_{01}). Moreover, Resonators 3 and 4 are used to construct the passband for Channel II, and their fundamental resonant frequency corresponds to the center frequency of Channel II (f_{02}). Both channels exhibit second-order Chebyshev bandpass responses. Notably, all resonators are diode-loaded; thus, their resonant frequencies can be adjusted by applying an external bias. When the resonant frequency of a resonator matches the center frequency of the passband, signals within the frequency band are allowed to pass, thus placing the passband in the ON state. Conversely, when the resonant frequency of the resonator changes to a value that is not within the passband, the resonator provides signal rejection, thereby causing the passband to be in the OFF state. Furthermore, the proposed design method involves the application of distributed coupling technology, thus obviating the need for additional matching circuits. Consequently, the overall circuit size can be substantially reduced. Furthermore, in the proposed design method, the loading effect between different frequency bands is minimal; thus, each passband can be designed independently and then integrated. Notably, the proposed design method enhances structural flexibility because it allows increases in filter order and channel number through the addition of more resonators or filter units, respectively.

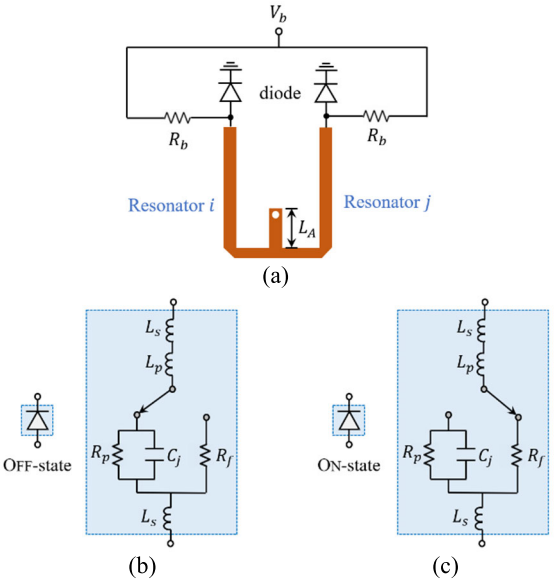

FIGURE 3. (a) Schematic of microstrip diode-loaded coupled resonators. (b) ON-state and (c) OFF-state equivalent circuits of a p–i–n diode.

To facilitate circuit miniaturization, diode-loaded quarter-wavelength ($\lambda/4$) resonators can be used. Fig. 3(a) illustrates the microstrip-line structure of such coupled resonators; the circuit comprises two diode-loaded $\lambda/4$ resonators, which are denoted as i and j. To facilitate miniaturization, these two resonators share the same short-circuited stub section.

TABLE 1. Operating modes of a filtering diplexer integrated with SPDT switches.

Operating modes	States	
Mode 1 (Switchable BPF @ f_{01})	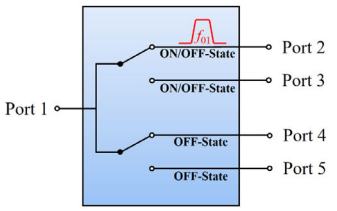	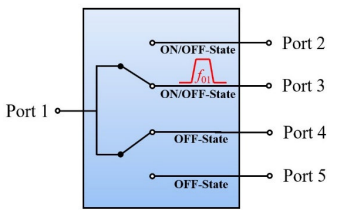
Mode 2 (Switchable BPF @ f_{02})	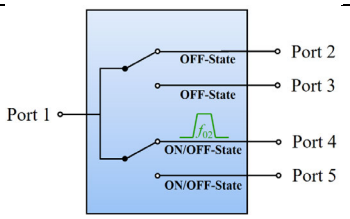	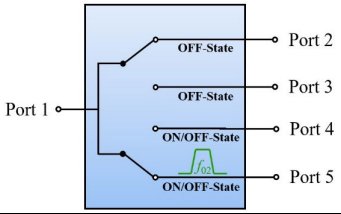
Mode 3 (Switchable diplexer @ f_{01} and f_{02})	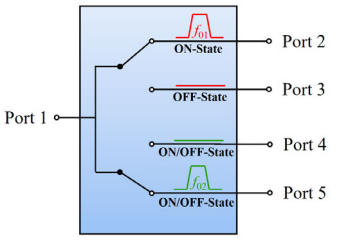	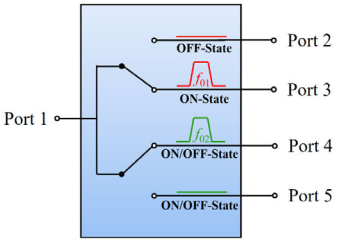
	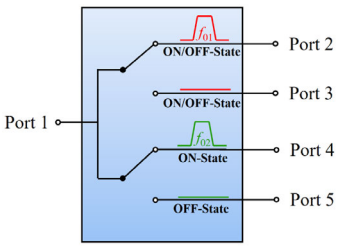	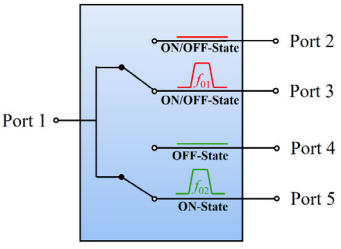

Moreover, the coupling coefficient between these resonators can be controlled by adjusting the length of this short-circuited stub, which is denoted as L_A in Fig. 3(a) [28]. Each of these two resonators has a p–i–n diode connected to its open-circuit end. When a reverse bias is applied to the diodes, the diodes are all at OFF-state and each resonator is effectively equivalent to a $\lambda/4$ resonator operating at the center frequency of the channel passband; thus, the channel passband can be turned on. Conversely, when a forward bias is applied to the diodes, the diodes are all at ON-state and the resonant frequency of each resonator doubles the center frequency; therefore, the channel passband can be turned off. An Infineon BAR65-02V p–i–n diode can be used in the implementation process; its equivalent circuits at ON-state and OFF-state are displayed in Fig. 3(b) and (c), respectively, in which the parasitic inductance is $L_s = 0.9$nH, the capacitance is $C_j = 0.37$pF, the resistance under forward bias is $R_f = 1\Omega$, and the resistance under reverse bias is $R_p = 7000\Omega$. When external bias voltages of 1 V and -30 V are applied, this diode can be turned on and off, respectively. Notably, to compensate for the parasitic inductance from the diodes, slight adjustments in resonator dimensions are required to maintain the originally specified resonant frequency.

TABLE 2. Specifications of the designed second-order filtering diplexer integrated with SPDT switches.

	Channel I	Channel II
Center frequency (GHz)	1.48	2.02
Bandwidth (MHz)	80	65
Filter order	2	2
Frequency response	Chebyshev (0.04321-dB ripple)	

To validate the aforementioned design concept, this study designed and implemented a second-order Chebyshev filtering diplexer integrated with SPDT switches. A Rogers RO4003 substrate with a dielectric constant of 3.55, a thickness of 32 mil (0.8128 mm), and a loss tangent of 0.0027 was used. The design specifications are presented in Table 2. The microstrip layout of the second-order filtering diplexer integrated with SPDT switches is

displayed in Fig. 4. The circuit of this diplexer comprised eight diode-loaded $\lambda/4$ resonators. All first-stage resonators were appropriately placed along the input feeding coupled line. In the ON state (when the diodes were turned off), Resonators 1^A, 2^A, 1^B, and 2^B exhibited a resonant frequency of 1.48 GHz, whereas Resonators 3^A, 4^A, 3^B, and 4^B exhibited a resonant frequency of 2.02 GHz. Because a distributed coupling structure was used in the aforementioned circuit, the loading effects between different channels were extremely weak. Therefore, frequency bands for all channels could be designed independently, which indicates that the proposed method is relatively straightforward and offers flexibility in passband design.

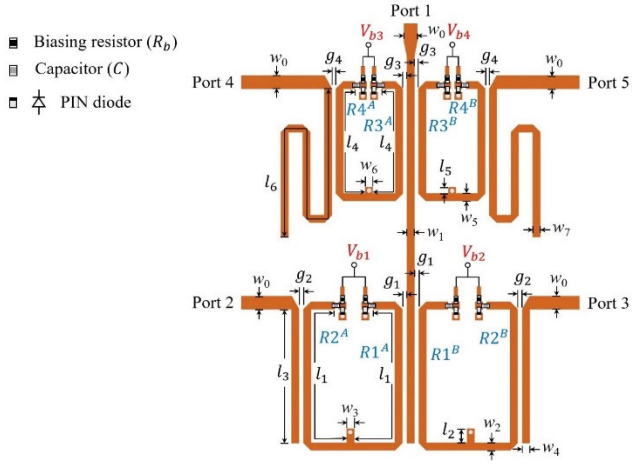

FIGURE 4. Layout of the second-order filtering diplexer integrated with SPDT switches (C = 100 pF; R_b= 10kΩ).

The required coupling coefficients and input/output (I/O) external quality factors for a Chebyshev BPF can be determined on the basis of the values of the elements of the corresponding low-pass prototype circuit and the specified fractional bandwidth, as expressed in the following equations [29]:

$$M_{m,m+1} = \frac{FBW}{\sqrt{g_m g_{m+1}}} \tag{1}$$

$$Q_e = \frac{g_0 g_1}{FBW} \tag{2}$$

where FBW represents the fractional bandwidth and g represents the values of the elements of the low-pass prototype circuit. On the basis of the provided specifications, this study determined the following theoretical values for the coupling coefficients and I/O external quality factors: $M^I_{12} = 0.09$, $M^{II}_{34} = 0.053$, $Q^I_{ei} = Q^I_{eo} = 12.3$, and $Q^{II}_{ei} = Q^{II}_{eo} = 20.8$.

Next, this study experimentally determined the coupling coefficients and external quality factors for the implemented circuit. In the designed circuit, the coupling coefficient is controlled by the length of the shared short-circuited stub (l_2 and l_5). For synchronously tuned coupled-resonator circuits, the relationship between coupling coefficients and resonant frequencies can be expressed as follows:

$$M = \pm\frac{f_{p2}^2 - f_{p1}^2}{f_{p2}^2 + f_{p1}^2} \tag{3}$$

where f_{p1} and f_{p2} denote the lower and upper resonant frequencies of the two coupled resonators, respectively; the sign of the coupling coefficient depends on the specific coupling structure and its phase variation. In addition, the external quality factor is controlled by the spacing (g_1, g_2, g_3, and g_4), line width (w_1, w_4, and w_7), and length of the I/O coupled lines (l_3 and l_6). The external quality factor can be expressed as follows:

$$Q_e = \frac{\pi f_0 \tau_d(f_0)}{2} \tag{4}$$

where $\tau_d(f_0)$ represents the group delay at the center frequency f_0. Fig. 5(a) and (b) show the calculated results for coupling coefficient and the external quality factor, respectively. When the extracted coupling coefficients and external quality factors meet their theoretical values, the physical parameters of the diplexer can be determined.

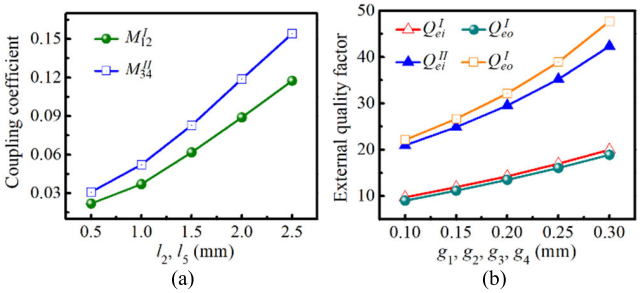

FIGURE 5. Design curves for the second-order filtering diplexer integrated with SPDT switches. (a) Extracted coupling coefficients and (b) extracted external quality factors. (w_1=w_4=w_7= 1 mm, l_3= 18.5 mm, and l_6= 47.5mm).

TABLE 3. Physical parameters of the fabricated second-order filtering diplexer integrated with SPDT switches. (unit: mm).

l_1	l_2	l_3	l_4	l_5	l_6
27.16	1.97	18.5	19.5	1.0	47.5
w_0	w_1	w_2	w_3	w_4	w_5
1.8	1.0	1.0	1.0	1.0	1.0
w_6	w_7	g_1	g_2	g_3	g_4
1.0	1.0	0.16	0.16	0.1	0.1

The current distribution of the second-order filtering diplexer integrated with SPDT switches in Fig. 6 illustrates minimal loading effects between different frequency bands, and each channel passband can be independently switched on or off. A photograph of the fabricated second-order filtering diplexer integrated with SPDT switches is depicted in Fig. 7. All physical parameters for this diplexer are listed in Table 3. Please note that, to satisfy the required external coupling, gaps g_1, g_2, g_3, and g_4 are maintained at values close to the minimums permitted by the PCB technology.

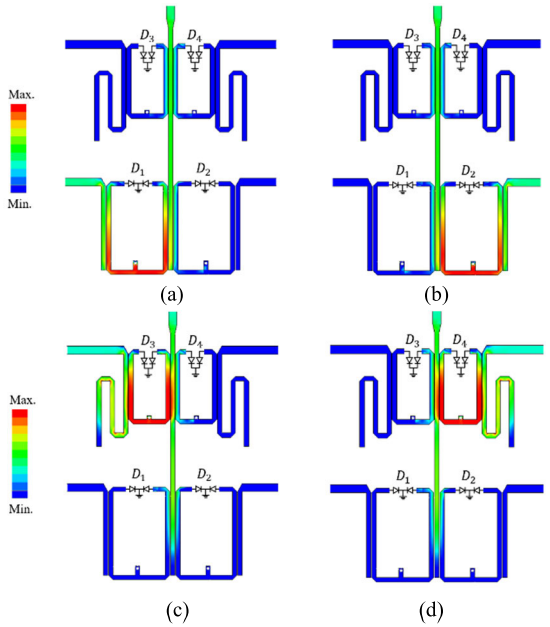

FIGURE 6. Current distribution of the second-order filtering diplexer integrated with SPDT switches. (a) 1.48 GHz (D_1 OFF and D_2 ON). (b) 1.48 GHz (D_2 OFF and D_1 ON). (c) 2.02 GHz (D_3 OFF and D_4 ON). (d) 2.02 GHz (D_4 OFF and D_3 ON).

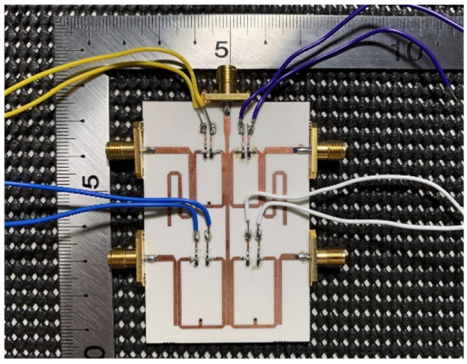

FIGURE 7. Photograph of the fabricated second-order filtering diplexer integrated with SPDT switches.

If there is a requirement for increased coupling strength (or bandwidth), it is advisable to consider opting for a thicker substrate in the design. The circuit size of this multifunctional diplexer was determined to be 33.8 mm × 51.8 mm, which is equivalent to only $0.25\lambda_g \times 0.39\lambda_g$ (i.e., $0.098\lambda_g^2$), where λ_g is the guided wavelength at 1.48 GHz. Simulation and experimental results obtained for the second-order filtering diplexer integrated with SPDT switches are illustrated in Fig. 8, 9, and 10; the simulation and experimental results were verified using the Advanced Design System full-wave EM simulation software program and an Agilent N5230A vector network analyzer, respectively. The dashed lines in these figures represent the simulation results, and the solid lines represent the measurement results. When a reverse bias was applied to V_{b1} and forward biases were applied to V_{b2}, V_{b3}, and V_{b4}, the operating mode switched to Mode 1 [Fig. 8(a) and (b)]. In this mode, the circuit operated as a second-order SPDT switchable BPF with a center frequency of 1.48 GHz, and signals were output from Port 2. Conversely, when a reverse bias was applied to V_{b2} and forward biases were applied to V_{b1}, V_{b3}, and V_{b4}, the circuit operated as a second-order SPDT switchable BPF with a center frequency of 1.48 GHz, and signals were output from Port 3. When a reverse bias was applied to V_{b3} and forward biases were applied to V_{b1}, V_{b2}, and V_{b4}, the operating mode switched to Mode 2 [Fig. 9(a) and (b)]. In this mode, the circuit operated as a second-order SPDT switchable BPF with a center frequency of 2.02 GHz, and signals were output from Port 4. However, when a reverse bias was applied to V_{b4} and forward biases were applied to V_{b1}, V_{b2}, and V_{b3}, the circuit again operated as a second-order SPDT switchable BPF with a center frequency of 2.02 GHz, but signals were output from Port 5. Moreover,

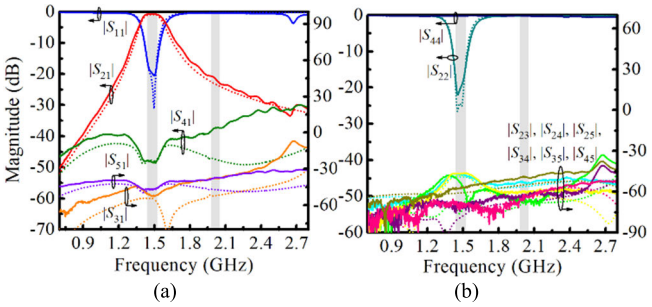

FIGURE 8. Simulation and experimental results for the first operating mode (Mode 1) of the second-order filtering diplexer integrated with SPDT switches. (a) $|S_{11}|$, $|S_{21}|$, $|S_{31}|$, $|S_{41}|$, and $|S_{51}|$. (b) $|S_{22}|$, $|S_{44}|$, $|S_{23}|$, $|S_{24}|$, $|S_{25}|$, $|S_{34}|$, $|S_{35}|$, and $|S_{45}|$.

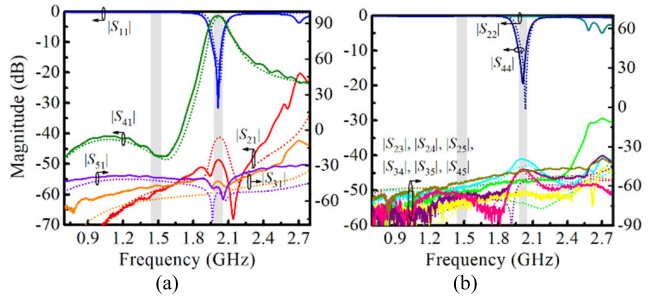

FIGURE 9. Simulation and experimental results for the second operating mode (Mode 2) of the second-order filtering diplexer integrated with SPDT switches. (a) $|S_{11}|$, $|S_{21}|$, $|S_{31}|$, $|S_{41}|$, and $|S_{51}|$. (b) $|S_{22}|$, $|S_{44}|$, $|S_{23}|$, $|S_{24}|$, $|S_{25}|$, $|S_{34}|$, $|S_{35}|$, and $|S_{45}|$.

when reverse biases were applied to V_{b1} and V_{b3} and forward biases were applied to V_{b2} and V_{b4}, one of the diplexer modes (i.e., Mode 3) was achieved [Fig. 10(a) and (b)]. In this mode, second-order filter responses with center frequencies of 1.48 and 2.02 GHz were output from Ports 2 and 4, respectively. Note that, if forward biases were applied to V_{b1}, V_{b2}, V_{b3}, and V_{b4}, a full OFF-state mode with simultaneous no transmission at both bands can be achieved.

When the passband was turned on, the measured return losses (i.e., $-20\log|S_{11}|$) within the channel passbands were

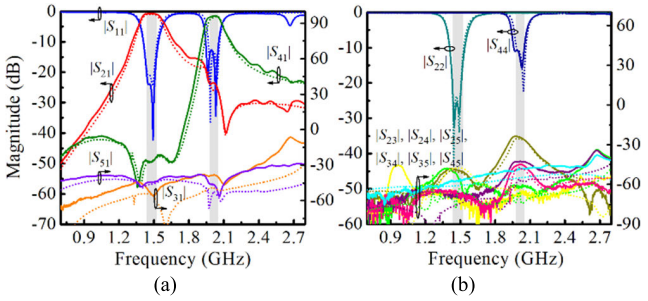

FIGURE 10. Simulation and experimental results for the third operating mode (Mode 3) of second-order filtering diplexer integrated with SPDT switches. (a)$|S_{11}|$, $|S_{21}|$, $|S_{31}|$, $|S_{41}|$, and $|S_{51}|$. (b) $|S_{22}|$, $|S_{44}|$, $|S_{23}|$, $|S_{24}|$, $|S_{25}|$, $|S_{34}|$, $|S_{35}|$, and $|S_{45}|$.

> 13 dB. Moreover, the in-band insertion losses (i.e., $-20\log|S_{21}|$ and $-20\log|S_{41}|$) for Channels I and II were approximately 0.68 and 1.45 dB, respectively, which can be primarily attributed to conductor loss. When the passband was turned off, the attenuations within the operational frequency bands for Channels I and II were > 60 and > 42 dB, respectively. Furthermore, in Mode 3 (diplexer mode), the isolation between the output ports for Channels I and II (i.e., $-20\log|S_{24}|$) was 48 dB, and the isolations between the other output ports (i.e., $-20\log|S_{23}|$, $-20\log|S_{25}|$, $-20\log|S_{34}|$, $-20\log|S_{35}|$, and $-20\log|S_{45}|$) were > 25 dB.

III. DIPLEXERS INTEGRATED WITH SPDT SWITCHES AND EXHIBITING FOURTH-ORDER BANDPASS RESPONSES

The proposed method can also be used to design a fourth-order filtering diplexer integrated with SPDT switches that has enhanced selectivity. The coupling structure of such a diplexer is illustrated in Fig. 11, where Nodes $1^A - 8^A$ and $1^B - 8^B$ represent resonators, and Nodes S and L represent the source and load, respectively. In Fig. 11, the solid lines between the nodes indicate the coupling paths. All resonators in the aforementioned structure are diode-loaded resonators. Resonators 1–4 are used to create the passband for Channel I, and their resonance frequencies correspond to the center frequency of Channel I (f_{01}). Resonators 5–8 are used to construct the passband for Channel II, and their resonance frequencies correspond to the center frequency of Channel II (f_{02}). Both channels exhibit fourth-order Chebyshev bandpass responses.

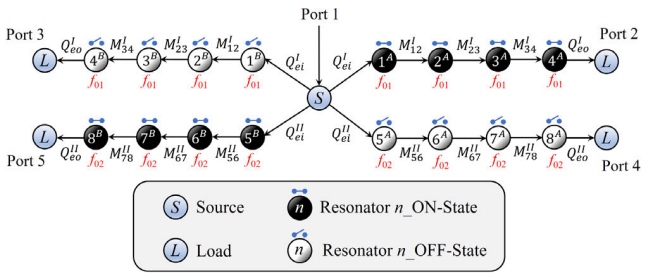

FIGURE 11. Coupling structure of the fourth-order filtering diplexer integrated with SPDT switches.

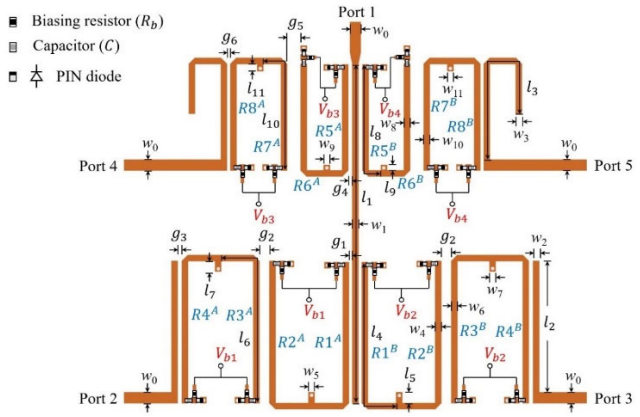

FIGURE 12. Layout of the designed fourth-order filtering diplexer integrated with SPDT switches (C = 100 pF; R_b= 10 kΩ).

TABLE 4. Specifications of the fourth-order filtering diplexer integrated with SPDT switches.

	Channel I	Channel II
Center frequency (GHz)	1.44	2.04
Bandwidth (MHz)	132	130
Filter order	4	4
Frequency response	Chebyshev (0.04321-dB ripple)	

To validate the aforementioned design concept, this study implemented a fourth-order multifunctional diplexer on a Rogers RO4003 substrate with a thickness of 32 mil (0.8128 mm). The design specifications are listed in Table 4. The microstrip structure of this multifunctional diplexer is displayed in Fig. 12, and this structure contained two pairs of fourth-order SPDT switchable BPFs. Each SPDT switchable BPF comprised four diode-loaded $\lambda/4$ resonators. The couplings between the first- and second-stage resonators (M_{12} and M_{56}), in addition to those between the third- and fourth-stage resonators (M_{34} and M_{78}), could be controlled by varying the length of the shared short-circuited stub (l_5, l_7, l_9, and l_{11}). In general, when the length of the short-circuited stub is greater, the coupling coefficient between the resonators is higher; Furthermore, the couplings between the second- and third-stage resonators (M_{23} and M_{67}) could be controlled by varying the spacing between them (g_2 and g_5). In general, when this spacing is smaller, the coupling coefficient between the resonators is higher. Moreover, the external quality factor can be controlled by varying the spacing (g_1, g_3, g_4, and g_6), line width (w_1, w_2, and w_3), and length of the input and output coupled lines (l_2 and l_3). In general, when the spacing between coupled lines is smaller, the line width is narrower, the coupled lines are longer, and the external loaded quality factor is smaller. This study derived the following theoretical values for the required coupling coefficients and I/O external quality factors of the implemented multifunctional diplexer: $M^I_{12} = M^I_{34} = 0.084$, $M^I_{23} = 0.064$, $M^{II}_{56} = M^{II}_{78} = 0.06$, $M^{II}_{67} = 0.046$, $Q^I_{ei} = Q^I_{eo} = 10.1$, and $Q^{II}_{ei} = Q^{II}_{eo} = 14.1$. Similarly, to reduce

the circuit size and improve the stopband response, diode-loaded $\lambda/4$ resonators were used. Furthermore, on the basis of the distributed coupling structure, the frequency bands for all channels could be individually designed without the need for additional matching circuits. This feature not only simplified the design but also contributed to miniaturization. Fig. 13(a), (b), and (c) show the calculated results for coupling coefficient and the external quality factor. Also, when the extracted coupling coefficients and external quality factors meet their theoretical values, the physical parameters of the diplexer can be determined.

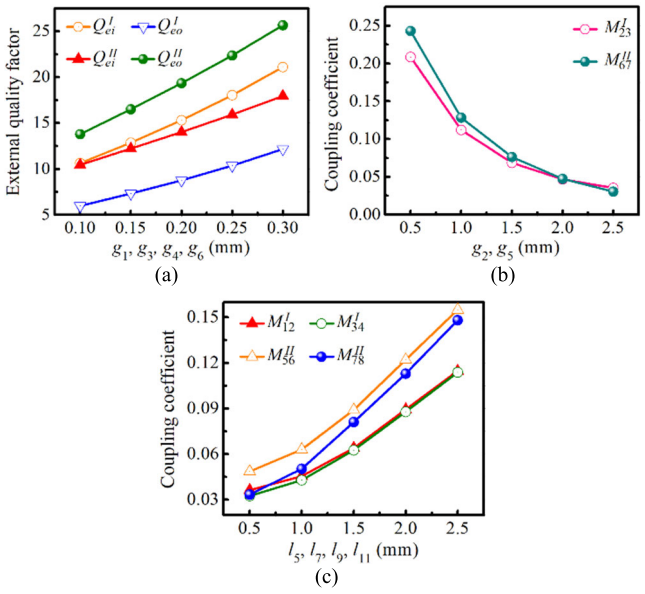

FIGURE 13. Design curves for the fourth-order filtering diplexer integrated with SPDT switches. (a) Extracted coupling coefficients and (b) extracted external quality factors. (w_1=w_2=w_3= 1 mm, l_2= 22.2 mm, and l_3= 29 mm).

The current distribution of the fourth-order filtering diplexer integrated with SPDT switches is shown in Fig. 14.

TABLE 5. Physical parameters of the implemented fourth-order filtering diplexer integrated with SPDT switches. (unit: mm).

l_1	l_2	l_3	l_4	l_5	l_6
57.2	22.2	29	28.6	1.82	29.5
l_7	l_8	l_9	l_{10}	l_{11}	w_0
1.78	20	0.91	21	1.31	1.8
w_1	w_2	w_3	w_4	w_5	w_6
1.0	1.0	1.0	1.0	1.0	1.0
w_7	w_8	w_9	w_{10}	w_{11}	g_1
1.0	1.0	1.0	1.0	1.0	0.1
g_2	g_3	g_4	g_5	g_6	
1.72	0.25	0.22	2.34	0.11	

It also indicates that each channel passband can be independently switched on or off. A photograph of the implemented fourth-order filtering diplexer integrated with SPDT switches is depicted in Fig. 15. All physical parameters of this diplexer are listed in Table 5. The circuit size of this multifunctional diplexer was 60 mm × 59.3 mm, which was determined to be equivalent to only $0.44\lambda_g \times 0.44\lambda_g$(i.e., $0.198\lambda_g^2$), where λ_g is the guided wavelength at 1.44 GHz. Simulation and experimental results derived for

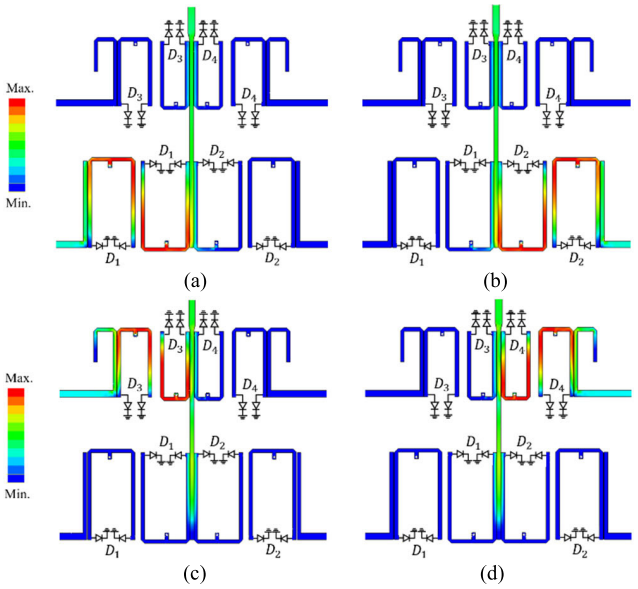

FIGURE 14. Current distribution of the fourth-order filtering diplexer integrated with SPDT switches. (a) 1.44 GHz (D_1 OFF and D_2 ON). (b) 1.44 GHz (D_2 OFF and D_1 ON). (c) 2.04 GHz (D_3 OFF and D_4 ON). (d) 2.04 GHz (D_4 OFF and D_3 ON).

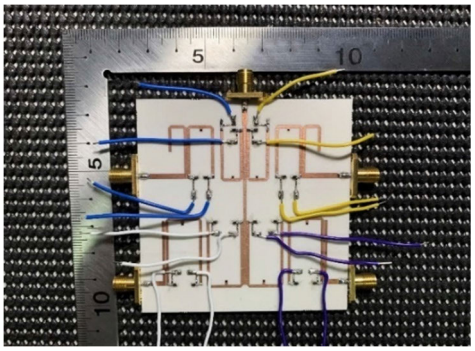

FIGURE 15. Photograph of the implemented fourth-order filtering diplexer integrated with SPDT switches.

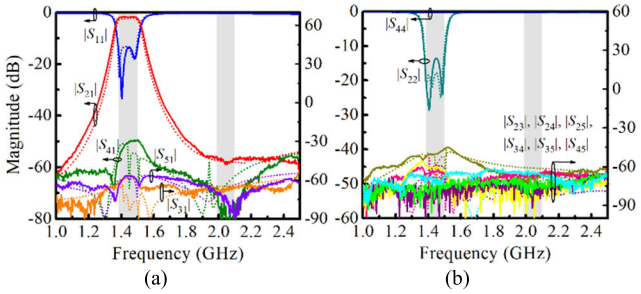

FIGURE 16. Simulation and experimental results for the first operating mode (Mode 1) of the fourth-order filtering diplexer integrated with SPDT switches. (a) $|S_{11}|$, $|S_{21}|$, $|S_{31}|$, $|S_{41}|$, and $|S_{51}|$. (b) $|S_{22}|$, $|S_{44}|$, $|S_{23}|$, $|S_{24}|$, $|S_{25}|$, $|S_{34}|$, $|S_{35}|$, and $|S_{45}|$.

TABLE 6. Comparison of implemented diplexers with state-of-the-art switchable diplexers.

	ON-state				OFF-state	Isolation (dB)	Design flexibility	Number of control voltages	Size (λ_g^2)
	Center frequency (GHz)	FBW (%)	IL (dB)	Order	Attenuation (dB)				
This work (1)	1.48, 2.02	5.4, 3.2	0.68, 1.45	2, 2	**60**, **42**	48	**High**	4	0.098
This work (2)	1.44, 2.04	9.2, 6.4	1.6, 2.5	4, 4	**70**, **65**	50	**High**	4	0.198
[15]	2, 2.8	10, 5	1.54, 2.6	4, 4	25, 40	30	Medium	2	~0.355
[16]	2, 2.2, 2.4, 2.6	0.4, 0.36, 0.33, 0.3	1.1, 1.4, 1.3, 1.5	2, 2, 2, 2	27, 23, 26, 21	30	Low	2	0.42
[17]	1.2, 1.5	3.5, 3	2.1, 2.21	2, 2	30, 30	40	High	2	0.029
[18]	0.8, 1	10, 10	1.16, 1.13	3, 3	45, 45	40	Medium	6	0.026
[19]	0.6, 0.9, 1.22, 1.58	3.6, 5.5, 5.7, 6	3.5, 3.1, 3.1, 2.9	3, 3	20, 20	55	Low	4	0.043
[20]	0.9, 1.25	14.5, 15	1.82, 1.98	4, 4	25, 25	51	Medium	4	0.054
[21]	2.35, 3.5	25, 28	1.3, 1.34	3, 3	20, 20	25	Low	5	0.039
[23]	2.05, 2.45	12, 13.7	1.13, 1.35	2, 2	32, 32	N/A	Medium	2	0.067
[27]	0.9, 1.8	9.2, 13.5	1.98, 1.45	4, 4	40, 35	34	Low	4	0.0378

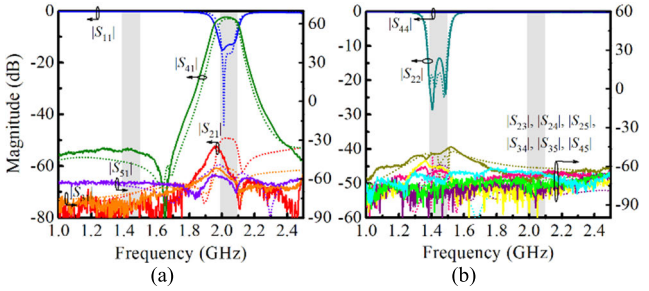

FIGURE 17. Simulation and experimental results for the second operating mode (Mode 2) of the fourth-order filtering diplexer integrated with SPDT switches. (a) $|S_{11}|$, $|S_{21}|$, $|S_{31}|$, $|S_{41}|$, and $|S_{51}|$. (b) $|S_{22}|$, $|S_{44}|$, $|S_{23}|$, $|S_{24}|$, $|S_{25}|$, $|S_{34}|$, $|S_{35}|$, and $|S_{45}|$.

the implemented fourth- order filtering diplexer are depicted in Fig. 16, 17, and 18. In these figures, the dashed lines represent the simulation results, and the solid lines represent the experimental results. When a reverse bias was applied to V_{b1} and forward biases were applied to V_{b2}, V_{b3}, and V_{b4}, the operating mode switched to Mode 1 [Fig. 16(a) and (b)]. In this mode, the circuit operated as a fourth-order SPDT switchable BPF with a center frequency of 1.44 GHz, and signals were output from Port 2. Conversely, when a reverse bias was applied to V_{b2} and forward biases were applied to V_{b1}, V_{b3}, and V_{b4}, a fourth-order filter response at a center frequency of 1.44 GHz was output from Port 3. When a reverse bias was applied to V_{b3} and forward biases were applied to V_{b1}, V_{b2}, and V_{b4}, the operating mode switched to Mode 2 [Fig. 17(a) and (b)]. In this mode, the circuit operated as a fourth-order SPDT switchable BPF with a center frequency of 2.04 GHz, and signals were output from Port 4. Conversely, when a reverse bias was applied to V_{b4} and forward biases were applied to V_{b1}, V_{b2}, and V_{b3}, a fourth-order filter response at a center frequency of 1.44 GHz was output from Port 5. However, when reverse biases were applied to V_{b1} and V_{b3} and forward biases were applied to V_{b2} and V_{b4}, one of the diplexer modes (i.e., Mode 3) could be achieved [Fig. 18(a) and (b)]. In this mode, fourth-order filter responses with center frequencies of 1.44 and 2.04 GHz were output from Ports 2 and 4, respectively. Please be aware that applying forward biases to V_{b1}, V_{b2}, V_{b3}, and V_{b4} can result in a full OFF-state mode, simultaneously preventing transmission at both bands.

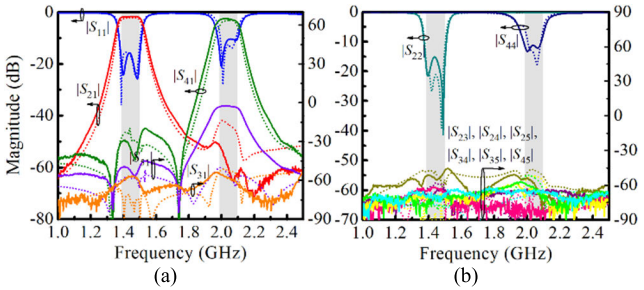

FIGURE 18. Simulation and experimental results for the third operating mode (Mode 3) of the fourth-order filtering diplexer integrated with SPDT switches. (a)$|S_{11}|$, $|S_{21}|$, $|S_{31}|$, $|S_{41}|$, and $|S_{51}|$. (b) $|S_{22}|$, $|S_{44}|$, $|S_{23}|$, $|S_{24}|$, $|S_{25}|$, $|S_{34}|$, $|S_{35}|$, and $|S_{45}|$.

When the passband was in the ON state, the measured in-band return losses were $>$ 10 dB, and the insertion losses within the 1.44- and 2.04-GHz bands were approximately 1.6 and 2.5 dB, respectively; these insertion losses are primarily attributed to conductor losses. When the passband was in the OFF state, the measured attenuations exceeded 70 and 65 dB within the 1.44- and 2.04-GHz bands, respectively. In addition, in Mode 3 (diplexer mode), the isolation between the output ports of Channels I and II was $>$ 50 dB, and the isolation between the other output ports was $>$ 45 dB. Accordingly, the full-wave EM

simulations and the experimental results were consistent, which validated the feasibility of the proposed method for designing filtering diplexers integrated with SPDT switches. The comparison of the implemented diplexers with state-of-the-art switchable diplexers is summarized in Table 6. It can be observed that the proposed diplexers demonstrates higher degree of design flexibility with satisfactory performance. Besides, the proposed diplexers provides three switchable operating modes, and are suitable for TDD and FDD systems.

IV. CONCLUSION

This paper presents a novel design method for multifunctional filtering diplexers integrated with SPDT switches. Such multifunctional diplexers can operate in three modes: Modes 1–3. Modes 1 and 2 involve the operation of switchable BPFs at different frequencies, and these BPFs are suitable for TDD systems. Mode 3 involves the operation of a switchable diplexer, which is suitable for TDD and FDD systems. This study validated the feasibility and flexibility of the proposed design method by using it to develop second- and fourth-order multifunctional diplexers; this study assessed the developed diplexers through EM simulations and experimental measurements. The EM simulation results were in good agreement with the experimental results. In summary, the proposed design method for multifunctional filtering diplexers integrated with SPDT switches offers advantages such as increased circuit compactness, improved performance, and enhanced design flexibility; therefore, this method is highly suitable for designing diplexers for modern multiband TDD and FDD communication systems.

REFERENCES

[1] S.-S. Oh and Y.-S. Kim, "A compact duplexer for IMT-2000 handsets using microstrip slow-wave open-loop resonators with high-impedance meander lines," in *Proc. IEEE Radio Wireless Conf. (RAWCON)*, Aug. 2001, pp. 177–180.

[2] G.-A. Lee, M. Megahed, and F. De Flaviis, "Design of multilayer spiral inductor resonator filter and diplexer for system-in-a-package," in *IEEE MTT-S Int. Microw. Symp. Dig.*, Jun. 2003, pp. 527–530.

[3] T. Yang, P.-L. Chi, and T. Itoh, "Compact quarter-wave resonator and its applications to miniaturized diplexer and triplexer," *IEEE Trans. Microw. Theory Techn.*, vol. 59, no. 2, pp. 260–269, Feb. 2011.

[4] P.-H. Deng, C. H. Chen, B.-L. Huang, J.-H. Jheng, H.-H. Tung, and P.-T. Chiu, "Design of wideband diplexer using broadside-coupled filters and stepped-impedance resonators," in *Proc. Asia–Pacific Microw. Conf.*, Dec. 2010, pp. 25–28.

[5] C.-F. Chen, T.-Y. Huang, C.-P. Chou, and R.-B. Wu, "Microstrip diplexers design with common resonator sections for compact size, but high isolation," *IEEE Trans. Microw. Theory Techn.*, vol. 54, no. 5, pp. 1945–1952, May 2006.

[6] T. Yang and G. M. Rebeiz, "Three-pole 1.3–2.4-GHz diplexer and 1.1–2.45-GHz dual-band filter with common resonator topology and flexible tuning capabilities," *IEEE Trans. Microw. Theory Techn.*, vol. 61, no. 10, pp. 3613–3624, Oct. 2013.

[7] C.-F. Chen, C.-Y. Lin, B.-H. Tseng, and S.-F. Chang, "High-isolation and high-rejection microstrip diplexer with independently controllable transmission zeros," *IEEE Microw. Wireless Compon. Lett.*, vol. 24, no. 12, pp. 851–853, Dec. 2014.

[8] T. Yang, P.-L. Chi, and T. Itoh, "High isolation and compact diplexer using the hybrid resonators," *IEEE Microw. Wireless Compon. Lett.*, vol. 20, no. 10, pp. 551–553, Oct. 2010.

[9] P.-H. Deng, M.-I. Lai, S.-K. Jeng, and C. H. Chen, "Design of matching circuits for microstrip triplexers based on stepped-impedance resonators," *IEEE Trans. Microw. Theory Techn.*, vol. 54, no. 12, pp. 4185–4192, Dec. 2006.

[10] J.-Y. Wu, K.-W. Hsu, Y.-H. Tseng, and W.-H. Tu, "High-isolation microstrip triplexer using multiple-mode resonators," *IEEE Microw. Wireless Compon. Lett.*, vol. 22, no. 4, pp. 173–175, Apr. 2012.

[11] S.-F. Chao, C.-H. Wu, Z.-M. Tsai, H. Wang, and C. H. Chen, "Electronically switchable bandpass filters using loaded stepped-impedance resonators," *IEEE Trans. Microw. Theory Techn.*, vol. 54, no. 12, pp. 4193–4201, Dec. 2006.

[12] W.-H. Tu, "Switchable microstrip bandpass filters with reconfigurable on-state frequency responses," *IEEE Microw. Wireless Compon. Lett.*, vol. 20, no. 5, pp. 259–261, May 2010.

[13] C.-S. Chen, J.-F. Wu, and Y.-S. Lin, "Compact single-pole-double-throw switchable bandpass filter based on multicoupled line," *IEEE Microw. Wireless Compon. Lett.*, vol. 24, no. 2, pp. 87–89, Feb. 2014.

[14] J. Xu, F. Liu, and Z.-Y. Feng, "Single-/dual-band bandpass filter-integrated single-pole double-throw switch using distributed coupling tri-mode resonators," *IEEE Trans. Microw. Theory Techn.*, vol. 68, no. 2, pp. 741–749, Feb. 2020.

[15] Y.-S. Lin, P.-C. Wang, C.-W. You, and P.-Y. Chang, "New designs of bandpass diplexer and switchplexer based on parallel-coupled bandpass filters," *IEEE Trans. Microw. Theory Techn.*, vol. 58, no. 12, pp. 3417–3426, Dec. 2010.

[16] M.-L. Chuang and M.-T. Wu, "Microstrip multiplexer and switchable diplexer with joint T-shaped resonators," *IEEE Microw. Wireless Compon. Lett.*, vol. 24, no. 5, pp. 309–311, May 2014.

[17] S.-C. Weng, K.-W. Hsu, and W.-H. Tu, "Switchable and high-isolation diplexer with wide stopband," *IEEE Microw. Wireless Compon. Lett.*, vol. 24, no. 6, pp. 373–375, Jun. 2014.

[18] C. Chen and Y. Lin, "Single-pole double-throw switchable diplexer and single-pole quadruple-throw switchable quadplexer using capacitively loaded multicoupled line," *IET Microw., Antennas Propag.*, vol. 9, no. 14, pp. 1547–1557, Nov. 2015.

[19] C.-F. Chen, B.-H. Tseng, and S.-F. Chang, "A compact and high isolation microstrip switchable diplexer," in *Proc. Asia–Pacific Microw. Conf. (APMC)*, Dec. 2015, pp. 1–3.

[20] J. Xu, "Compact switchable bandpass filter and its application to switchable diplexer design," *IEEE Microw. Wireless Compon. Lett.*, vol. 26, no. 1, pp. 13–15, Jan. 2016.

[21] X. Bi, Q. Ma, C. Ning, and Q. Xu, "A compact switchable filtering diplexer based on reused L-shaped resonator," *IEEE Trans. Circuits Syst. II, Exp. Briefs*, vol. 65, no. 12, pp. 1934–1938, Dec. 2018.

[22] C.-F. Chen, R.-Y. Chen, K.-W. Zhou, and Y.-H. He, "Microstrip switchable diplexer based on dual-mode stub-loaded stepped-impedance resonators with three operating states," *Electron. Lett.*, vol. 55, no. 22, pp. 1188–1190, Oct. 2019.

[23] J.-X. Xu, W.-L. Zhan, H.-Y. Li, and X. Y. Zhang, "Switchable diplexer based on coupling control," *IEEE Trans. Circuits Syst. II, Exp. Briefs*, vol. 68, no. 1, pp. 166–170, Jan. 2021.

[24] S. Weng, K. Hsu, and W. Tu, "Microstrip bandpass single-pole quadruple-throw switch and independently switchable quadruplexer," *IET Microw., Antennas Propag.*, vol. 8, no. 4, pp. 244–254, Mar. 2014.

[25] C. Chen, B. Tseng, G. Wang, and J. Li, "Compact microstrip eight-channel multiplexer with independently switchable passbands," *IET Microw., Antennas Propag.*, vol. 12, no. 6, pp. 1026–1033, May 2018.

[26] J. Xu, Z.-Y. Chen, and H. Wan, "Lowpass–bandpass triplexer integrated switch design using common lumped-element triple-resonance resonator technique," *IEEE Trans. Ind. Electron.*, vol. 67, no. 1, pp. 471–479, Jan. 2020.

[27] J. Xu, F. Liu, Z.-Y. Feng, and Y.-F. Guo, "Diplexer-integrated SPDT switches with multiple operating modes using common fractal stub-loaded resonator," *IEEE Trans. Microw. Theory Techn.*, vol. 69, no. 2, pp. 1464–1473, Feb. 2021.

[28] S.-C. Lin, "Microstrip dual/quad-band filters with coupled lines and quasi-lumped impedance inverters based on parallel-path transmission," *IEEE Trans. Microw. Theory Techn.*, vol. 59, no. 8, pp. 1937–1946, Aug. 2011.

[29] J. S. Hong and M. J. Lancaster, *Microstrip Filter for RF/Microwave Application*. New York, NY, USA: Wiley, 2001.

CHI-FENG CHEN (Member, IEEE) received the M.S. degree in electrophysics from National Chiao Tung University, Hsinchu, Taiwan, in 2003, and the Ph.D. degree in communication engineering from National Taiwan University, Taipei, Taiwan, in 2006.

From 2008 to 2010, he was an RF Engineer with Compal Communications Inc., Taipei, where he was involved in the research and development of global system for mobile communication (GSM) and code division multiple access (CDMA) mobile phones. In April 2010, he joined the Graduate Institute of Communication Engineering, National Taiwan University, as a Postdoctoral Research Fellow. Since 2012, he has been a Faculty Member with the Department of Electrical Engineering, Tunghai University (THU), Taichung, Taiwan, where he is currently a Professor. He is also the Chairperson of the Department of Electrical Engineering, THU. His research interests include the design of microwave circuits and associated RF modules for microwave and millimeter-wave applications.

YI-FANG TSAI was born in Yunlin, Taiwan, in 1978. She is currently pursuing the M.S. degree with the Department of Electrical Engineering, Tunghai University, Taichung, Taiwan. Her current research interest includes the design of RF/microwave circuits.

BAI-HONG CHEN was born in Taoyuan, Taiwan, in 1999. He is currently pursuing the M.S. degree with the Department of Electrical Engineering, Tunghai University, Taichung, Taiwan. His current research interest includes the design of RF/microwave circuits.

RUO-YIN YANG was born in Pingtung, Taiwan, in 1999. She is currently pursuing the M.S. degree with the Department of Electrical Engineering, Tunghai University, Taichung, Taiwan. Her current research interest includes the design of RF/microwave circuits.

YU-SHENG ZENG was born in Changhua, Taiwan, in 1998. He is currently pursuing the M.S. degree with the Department of Electrical Engineering, Tunghai University, Taichung, Taiwan. His current research interest includes the design of RF/microwave circuits.